Catalysis Science & Technology

ROYAL SOCIETY OF CHEMISTRY

PAPER

View Article Online
View Journal | View Issue

Cite this: *Catal. Sci. Technol.*, 2023, **13**, 4506

Enhanced coke-resistant Co-modified Ni/modified alumina catalyst for the bireforming of methane

Satyajit Panda,[ab] Vedant Joshi,[bc] Vivek Kumar Shrivastaw,[ab] Subhashis Das,[d] Mukesh Poddar,[a] Rajaram Bal [ab] and Ankur Bordoloi *[ab]

Received 28th March 2023,
Accepted 30th May 2023

DOI: 10.1039/d3cy00425b

rsc.li/catalysis

Biogas has been highlighted as a renewable energy and local source for syngas production *via* reforming techniques to combat global warming effects and energy sustainability. The bireforming of methane is one of the most suitable processes for utilizing biogas as it provides a syngas (H_2/CO) ratio of about 2, which is suitable to couple with downstream processes such as methanol and Fischer–Tropsch synthesis for the generation of liquid hydrocarbons. Metal–support interactions, surface acidity–basicity properties, and particle sizes play a pivotal role in reforming reactions. Herein, high surface area alumina was used with dopants ceria and magnesia, aiming to tune up the surface basicity and oxygen storage properties of the support. Over this, uniformly dispersed Ni and Co nanoparticles were synthesized *via* the deposition precipitation method. The doping of ceria and magnesia tuned the basicity of the support and showed an improved oxygen storage capacity favoring the inhibition of coke deposition and promoting catalyst activity and stability. The Ni–Co synergy not only provides a steady and excellent activity with conversion rates of 97% and 89% for CH_4 and CO_2 but also inhibits coke formation during 500 h long-term activity analysis.

1 Introduction

Energy security and environmental sustainability are the two greatest concerns of the present society, which has prompted the utilization of unexploited and sub-economic renewable energy resources. One of the most renewable, abundant, and clean energy sources, biogas can replace conventional fuels to produce thermal, electrical, and mechanical energy. Flexible feedstocks for biogas production comprise energy crops (*e.g.*, sugar beet, wheat, and sunflower), industrial wastes, wastewater, sewage sludge, municipal solid waste, agricultural residues, animal manure, and anaerobic digestion of biomass.[1,2] Moreover, the production of biogas and biogas plants is growing exponentially worldwide, which is encouraged by sustainable, climate, economic, and environmental welfare. The major challenge of biogas application is the widely distributed nature of biomass/waste materials that generate biogas, which is limited to lab-scale or pilot-scale reactors. Secondly, the transportation cost for the distribution to biogas from the feedstock hub location to the biogas feed reactor is high.[3]

Biogas primarily contains two global warming gases, namely, methane (50–70%) and carbon dioxide (20–40%), with trace amounts of other gases such as hydrogen, ammonia, hydrogen sulfide, oxygen, and nitrogen.[4–6] The presence of impurities and the typical biogas composition is another obstacle to its application, depending on the feedstocks used, which should be free from impurities, including nitrogen, sulfur species, siloxanes, and ammonia. Also, anaerobic digestion with different reaction conditions can control biogas content ratios.

Introducing reforming techniques for synthesizing syngas from biogas is an emerging strategy that dramatically influences the rapid climate change and depletion of petroleum-based sources. To date, three reforming processes have been developed, among which only the steam reforming of methane has been industrialized. Nevertheless, the technique has a limitation as the product contains an H_2/CO ratio of 3 : 1 and a substantial amount of CO_2, which will be difficult to use directly for either methanol synthesis or Fischer–Tropsch synthesis.[7] Dry methane reforming utilizes two major global warming gases, methane and carbon dioxide, in an equivalent ratio. However, due to the highly endothermic nature and rapid catalyst deactivation, the process is limited to the lab scale. In addition, syngas comes with a ratio close to 1, which is in a very low quantity and must be adjusted for further employment. Although the partial oxidation of methane can produce syngas with a desirable H_2/CO ratio of 2 for Fischer–Tropsch synthesis, a

[a] *Light and Stock Processing Division, CSIR-Indian Institute of Petroleum (IIP), Dehradun-248005, India. E-mail: ankurb@iip.res.in*
[b] *Academy of Scientific and Innovative Research (AcSIR), Ghaziabad-201002, India*
[c] *Polymeric Material Area, Chemical and Material Science Division, CSIR-Indian Institute of Petroleum (IIP), Dehradun-248005, India*
[d] *Department of Chemical Engineering, Institute of Chemical Technology, Nathalal Paresh Marg, Matunga, Mumbai-400019, India*

highly exothermic nature generates local hot spot[8] formation, fabricates explosions, and hinders its widespread application. In this scenario, bireforming, a combination of steam and dry reforming of methane,[7] is a practical approach and has the potential to produce a syngas mixture ratio of 2 : 1. Since it produces the syngas ratio of 2 : 1 straightforward manner with no additional purification and auxiliary separation of byproducts, it is an emerging approach for the reforming of biogas. Another advantage of this reaction is that the H_2/CO ratio can be controlled by adjusting the H_2O/CO_2 ratio to fulfill the downstream conditions.[9,10] In addition, from the thermodynamic point of view, carbon deposition in the case of bireforming is much lower than that in dry and oxyreforming.[11] Herein, both carbon dioxide and water are considered as oxidizing agents and help in the removal of deposited coke, due to which the catalytic activity and stability are enhanced.

$$\text{Steam Reforming of Methane: } CH_4 + H_2O \rightarrow CO + 3H_2 \quad \text{(i)}$$

$$\text{Dry Reforming of Methane: } CH_4 + CO_2 \rightarrow 2CO + 2H_2 \quad \text{(ii)}$$

$$\text{Bireforming of Methane: } 3CH_4 + CO_2 + 2H_2O \rightarrow 4CO + 8H_2 \quad \text{(iii)}$$

The primary reasons for coke deposition in the case of bireforming are the following reactions.

$$\text{Methane Decomposition } CH_4 \rightarrow 2H_2 + C \quad \text{(iv)}$$

$$\text{Boudward Reaction: } 2CO \rightarrow CO_2 + C \quad \text{(v)}$$

$$\text{Carbon Monoxide Hydrogenation: } CO + H_2 \rightarrow C + H_2O \quad \text{(vi)}$$

The equivalent activation of CH_4 and CO_2 is one of the major parameters for limiting coke deposition, which can be possible through metal–support interactions through catalyst surface structure and support acidity–basicity. The higher surface acidity of the support favors the cracking of methane and generates carbon, which encapsulates the metal atom and deactivates the catalyst. On the other hand, surface basicity prefers CO_2 dissociation, which produces more surface adsorbed oxygen that oxidizes the metal. Therefore, intermediate surface acidity–basicity with the good distribution of acidic and basic sites is one of the necessary requirements for bireforming. Group VIII elements and noble metals were widely investigated for the various reforming techniques of methane.[12] Moreover, Bian *et al.*[13] have proven that using Ni-based metal catalyst is the best alternative for reforming as it is readily available and economical. Iglauer and coworkers reviewed the use of Ni, Co, and Pt catalysts on various supports. Ni/γ-Al_2O_3 catalyst with a robust metal–support interaction showed long-term stability of 200 h at 850 °C and promising activity with a syngas ratio of 2.0 as well as 98% and 82% conversion of CH_4 and CO_2, respecctively.[14] Wang *et al.* used Ir-based catalyst during their methane activation studies and proved that unembedded Ir activates methane and the active oxygen species to convert CH_x intermediates, which favors a better CH_4 conversion.[15]

Bimetallic systems are introduced, aiming to have better catalytic performance and less coke deposition than monometallic system.[13] The better activity of bimetallics is correlated to the variation of active sites, complement & supplement of each other's advantages and synergetic effect-tuned electronic nature of metals. Furthermore, the higher binding nature of Co toward oxygen than Ni helps in CO_2 adsorption, which results in the metal particle oxidation and hence the easy removal of coke during the reaction.[16] On the other hand, Co-based catalysts, are very efficient toward soot oxidation, however, less active as compared to Ni based systems in BRM. Itkulova *et al.* used the bimetallic Co–Pt catalyst system for the bireforming of methane. They examined the response at 750 °C and obtained 100% methane conversion. Nonetheless, CO_2 conversion was significantly decreased during the reaction. Moreover, the magnetic behavior of Co might make it simpler to recycle the parent metal in a bimetallic system.[17]

Significantly, the support plays a pivotal role in thermal stability and catalytic activity, especially in reforming (dry, tri, & bi) reactions. With a large surface area, Al_2O_3 is the preferable support for reforming reactions because of mechanical strength, better textural properties, better dispersibility, and stability at higher temperatures. However, due to its acidic nature, coke deposition occurs very rapidly on its surface.[18] The doping of promoters to the support can control the acidity and limit coke deposition. Introducing alkaline earth oxides such as MgO can direct the support basicity and suppress the carbon formation by improving CO_2 adsorption.[19–21] The presence of magnesia also improves the CO_2 disproportionation rate. The base should be used in moderate quantity or else catalyst deactivation occurs through Boudward[22] and RWGS (reverse water gas shift) reaction.[19] Wei *et al.* revealed that ceria is the best option to be combined in alumina-supported Ni-based catalyst, particularly for reforming conditions.[23] Moreover, the added advantages of CeO_2 are: a. the redox nature, which helps enhance the catalyst's life span by oxidizing the deposited carbon as it has higher oxygen storage capacity;[22,24,25] b. improves the metal–support interaction; c. enhances the active phase dispersion;[25] and d. boosts the thermal stability of the support.[26] Ceria is one of the main interacting components of the support, which reacts with metal carbide to reactivate the catalyst. The reactions are as follows.[27]

$$CoC + 2CeO_2 \rightarrow Ce_2O_3 + Co + CO \quad -16.95 \text{ kcal mol}^{-1} \quad \text{(vii)}$$

$$NiC + 2CeO_2 \rightarrow Ce_2O_3 + Ni + CO \quad -7.63 \text{ kcal mol}^{-1} \quad \text{(viii)}$$

In addition to this, water behaves as a second oxidant in case of bireforming of methane. It restricts the coke deposition and controls H_2/CO ratio by changing the mole ratio. Therefore, a combination of these two (Ni and Co) metals over ceria and

magnesia-modified alumina support is supposed to increase the rate of CO_2 disproportionation and surface adsorbed oxygen species, which helps in carbon gasification reaction in a reduced environment with enhanced activity during long TOS study for bireforming.

Here, in this report, Ce–Mg doped high surface area alumina supported Ni–Co bimetallic catalyst was synthesized by a facile deposition precipitation method for the bireforming of methane. The catalyst's activities were examined in a fixed-bed reactor. Both fresh as well as spent materials have been exhaustively characterized with different experiments to elucidate the long-term stability with higher activity.

2 Experimental

2.1 Materials and reagents

Nickel nitrate hexahydrate and cobalt nitrate hexahydrate were purchased from SigmaAldrich Ltd. with 99.9% purity and AR grade. The customized 1% ceria and 3% magnesia-doped mesoporous alumina (mod alumina) has been prepared with the help of the method adopted from our earlier publications.[29,31] Double distilled water was used throughout the experiment, and methane, carbon dioxide, nitrogen, and hydrogen were purchased from Sigma gas services with a purity higher than 99.99%.

2.2 Deposition of active species 5% Ni and (1–5%) Co

The deposition–precipitation approach has been implemented to deposit the Ni and Co nanoparticles on the synthesized support by fixing the Ni weight percentage and varying the Co weight percentage (denoted as 5Ni–*x*Co mod alumina, x = 1 to 5). In a typical preparation approach, an aqueous solution of 0.82 g nickel nitrate hexahydrate and a stoichiometric amount of (according to weight percentage) cobalt nitrate hexahydrate were mixed at 60 °C and stirred for half an hour. 3 g dried surface-tuned alumina was poured into the Ni–Co mixture and stirred for another half an hour. Finally, urea was added into the metal–support mixture solution after a time gap of one hour and allowed to reflux at 90 °C for 48 h. The obtained precipitate was filtered and washed several times with distilled water, dried at 120 °C in a hot air oven for 12 h, followed by calcination at 850 °C for 6 h with a ramping rate of 1 °C min^{-1}.

The catalyst composition and abbreviation of the corresponding catalysts are described in Table 1. All the catalysts were prepared by following the same procedure described above.

Table 1 Catalyst composition and abbreviations

Catalyst composition	Abbreviation
5%Ni–1%Co–1%Ce–3%Mg–Al_2O_3	5Ni–1Co-mod alumina
5%Ni–2%Co–1%Ce–3%Mg–Al_2O_3	5Ni–2Co-mod alumina
5%Ni–3%Co–1%Ce–3%Mg–Al_2O_3	5Ni–3Co-mod alumina
5%Ni–4%Co–1%Ce–3%Mg–Al_2O_3	5Ni–4Co-mod alumina
5%Ni–5%Co–1%Ce–3%Mg–Al_2O_3	5Ni–5Co-mod alumina
5%Ni–1%Ce–3%Mg–Al_2O_3	5Ni-mod alumina
5%Co–1%Ce–3%Mg–Al_2O_3	5Co-mod alumina

2.3 Analytical measurements

The phase constitution of all the catalysts was determined using a Bruker D8 Advance X-ray diffractometer connected with a Lynx eye high-speed strip detector using CuKα radiation in the range of 2θ = 10–80°. The specific Brunauer–Emmett–Teller (BET) surface area of metal-loaded catalysts was calculated from N_2 adsorption–desorption isotherms at −180 °C using a Micromeritics ASAP 2020 surface & porosity analyzer. Barrett–Joyner–Halenda's (BJH) pore model was involved in pore size distribution investigation. The valence state of nickel and cobalt was performed by X-ray photoelectron spectroscopy (XPS) obtained using a Thermo Fisher Nexsa spectrometer equipped with monochromatic Al-Kα radiation with an energy of 1486.6 eV. The dual-beam charge neutralization was used for both low-energy electrons and ions. The powdered samples were mixed with IPA and sonicated for one minute and drop cast on the prefixed glass coverslips with two-sided carbon tape on the sample holders. Then, it was well-dried before loading in the load lock. Field emission scanning electron microscopy was carried out on an FEI Quanta 200F instrument to characterize the morphologies of the freshly prepared catalyst. The transmission electron microscopy (TEM) images of the samples were captured on an FEI Tecnai F30 transmission electron microscope. Before analysis, all the samples were well dispersed in ethanol for some time in a sonication bath and then mounted over a copper grid. Temperature programmed reduction (TPR), temperature-programmed desorption (TPD), and temperature programmed oxidation (TPO) were carried out using a Micromeritics Auto Chem II 2920 instrument having a temperature-controlled detector using helium as the carrier gas. For all the samples, exactly the same amount was analyzed to make comparison possible. Prior to measurements, the samples were degassed at 200 °C in an inert atmosphere (Helium UHP grade) for 2 h. The reducibility of the catalysts prepared in the current study was studied by the TPR technique in the temperature range of 100–1000 °C with 10 °C min^{-1} ramping rate using 10% H_2/balance He as the reactive gas. Thermogravimetric analyses and differential thermogravimetric (TGA & DTG) were performed using a TGA 4000 (PerkinElmer) instrument in nitrogen and zero air atmospheres from ambient temperature to 950 °C at a rate of 10 °C min^{-1}. Raman analysis was conducted on a Horiba Jobin Yvon dispersive microscope (HR800).

2.4 Investigation of catalytic performance for the bireforming of methane

The bireforming of methane was carried out in a fixed-bed continuous flow reactor (made of stainless steel with a length of 90 cm and inner diameter of 1.5 cm) at variant conditions. 2 g of each catalyst in the form of pellets (size = 850 micrometer) was held by quartz wool with a bilayer arrangement in the middle of the reactor, and ceramic beads

were used to form a fixed bed. The reactor was electrically heated in a split temperature-controlled furnace. Mass flow controllers were used for controlling the flow rate of CH_4, CO_2, N_2, and H_2, while the MX class liquid dosing pump regulated the accurate water flow. Before the reaction, all the samples were reduced at 850 °C with a flow rate of 100 mL min^{-1} with 20% H_2/N_2 for 2 h. The reactants were preheated to maintain the vapor phase and thoroughly mixed before reaching the catalyst bed. A cold trap was connected to the outlet of the reactor to isolate the unreacted water. The reaction was carried out with the reduced catalyst at different temperatures ranging from 650 to 850 °C. The weight hour space velocity (WHSV) was varied between 10 and 25 L g^{-1} h^{-1} with a molar ratio of $CO_2:H_2O:CH_4$ of 1:2:3. The reaction products were analyzed using an online gas chromatograph (Agilent 7890 A) fitted with a TCD detector using two different column molecular sieves, molecular sieve 5A (for analyzing H_2) and PoraPack-Q (for analyzing CH_4, CO_2, and CO).

Methane and carbon dioxide conversions were calculated according to eqn (ix) and (x), respectively. The syngas ratio (H_2/CO) was determined according to eqn (xi).

$$X_{CH_4}\ (\%) = \frac{F_{CH_4,in} - F_{CH_4,out}}{F_{CH_4,in}} \times 100 \quad \text{(ix)}$$

$$X_{CO_2}\ (\%) = \frac{F_{CO_2,in} - F_{CO_2,out}}{F_{CO_2,in}} \times 100 \quad \text{(x)}$$

$$\frac{H_2}{CO} = \frac{F_{H_2,out}}{F_{CO,out}} \quad \text{(xi)}$$

X_{CH_4} and X_{CO_2} are the conversions of methane and carbon dioxide, respectively. $F_{CH_4,in}$, $F_{CO_2,in}$, $F_{CH_4,out}$, $F_{CO_2,out}$, $F_{H_2,out}$, and $F_{CO,out}$ are the inlet and outlet flow of respective gases.

3 Results and discussion

3.1 Characterization of the fresh catalysts

The N_2 adsorption–desorption isotherms for the freshly synthesized catalysts are depicted in Fig. 1, and the textural parameter are provided in Table 2. According to the IUPAC classification, all the catalysts exhibit a type IV isotherm curve with an H1-type hysteresis loop,[28] typical of mesoporous materials with one-dimensional cylindrical channels. The considerable inflection at the partial pressures P/P_0 = 0.7–0.98 is attributed to the capillary condensation and N_2 desorption within the ordered mesopore, confirming the presence of a large mesopore and providing a high surface area. A high surface area of the synthesized catalysts offers a large area for the reactant molecule to be adsorbed, showing better catalytic activity. However, shifting the hysteresis loop toward lower P/P_0 partial pressure demonstrates the confinement of Ni–Co nanoparticles inside the mesopores.[29,30] Also, the pore volume and pore size rarely differ with a variation in cobalt weight percentage.

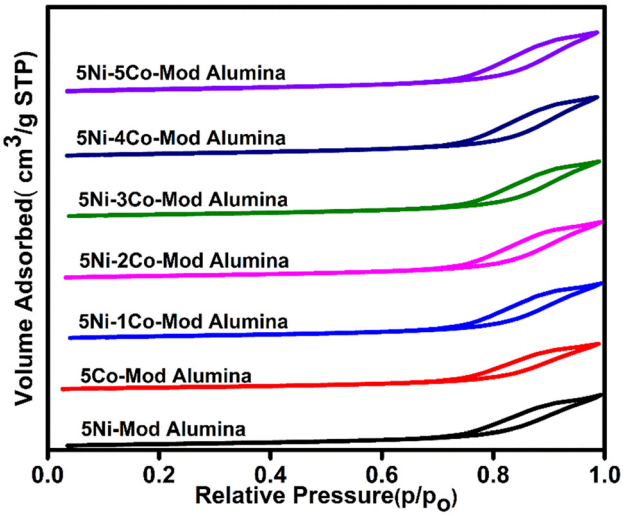

Fig. 1 N_2 adsorption–desorption isotherm profile of the freshly synthesized catalysts.

Fig. 2(a) and (b) represent the freshly synthesized catalyst XRD patterns in the region 2θ = 25–70°. The presence of three broad peaks at 37°, 46°, and 67° signifying the (311), (400), and (440) planes (JCPDS Card No. 77-1877) can be attributed to the $NiAl_2O_4$ phase. The peak broadening of the nickel aluminate phase signifies that a high temperature is needed to obtain a higher crystallinity of the specimen.[31,32] The diffraction peaks at 2θ = 31°, 37°, and 65° correspond to the (220), (311) & (440) plane (JCPDS Card No. 82-2252). Although the percentage of Ce and Mg is low, the peaks are observed due to the crystalline nature, with the combination of the aluminate phase. The 2θ value at 41°, 48°, and 60° confirm the presence of $CeAlO_3$ (JCPDS Card No. 81-11), and 19°, 36°, and 65° 2θ values confirm the presence of $MgAl_2O_4$ (JCPDS Card No. 77-1203).

The TPR profile after calcination at 850 °C is shown in Fig. 2(c). All the TPR patterns for bimetallic systems are similar and have a single broad reduction peak in the range of 800–850 °C. The peak is attributed to the reducing complex of nickel and cobalt oxide species. The reducibility of the active metal depends upon the degree of aggregation of metal oxides distributed on the support surface. A higher distribution of active metal leads to a stronger interaction and hence shifts the reduction peak to a higher reduction temperature region.[35] Another reason for the peak broadness is due to the collective formation of metal-aluminate species under higher calcination temperature,[31,36] and the results are concurrent with the XRD results. The hydrogen consumption is shown in Table 2. On the other hand, there is a single broad peak at about 700 °C for 5N-mod alumina and 5C-mod alumina, which may be due to the metal-aluminate phase formation.

To examine the effect of Ni & Co addition on the strength and distribution of basic sites, CO_2 temperature programmed desorption (TPD) studies were carried out. Fig. 2(d) shows the CO_2 TPD of the freshly synthesized catalyst, and the

Table 2 Surface area, total pore volume, and average pore diameter determined from N_2 adsorption–desorption isotherm of the freshly synthesized catalyst. Hydrogen consumption during H_2 TPR analysis. CO_2 TPD profile of the freshly synthesized catalysts

	Textural properties				CO_2 desorption values		
Catalyst	Average BET surface area ($m^2\ g^{-1}$)	Total pore volume ($cm^3\ g^{-1}$)	Average pore size (Å)	Hydrogen consumption (mmol g^{-1})	Weak signal (100–200 °C) (mmol g^{-1})	Strong signal (300–600 °C) (mmol g^{-1})	Total (mmol g^{-1})
5Ni–1Co-mod alumina	203	0.85	167	0.033	0.011	0.014	0.025
5Ni–2Co-mod alumina	204	0.84	167	0.054	0.007	0.012	0.019
5Ni–3Co-mod alumina	205	0.83	166	0.067	0.002	0.66	0.662
5Ni–4Co-mod alumina	209	0.82	163	0.075	0.009	0.031	0.040
5Ni–5Co-mod alumina	210	0.82	163	0.083	0.010	0.015	0.025
5Ni-mod alumina	235	0.79	155	1.25	0.000	0.108	0.108
5Co-mod alumina	228	0.80	158	1.39	0.000	0.105	0.105

amount of desorption is shown in Table 2. The CO_2 TPD profile of the bimetallic samples shows weak basic sites between 100 and 150 °C and strong sites in the range of 500–600 °C. The basic sites are due to the presence of promoter MgO in the support, which helps to adsorb more CO_2 and removal of coke from the active sites of the catalyst by providing a number of oxygen molecules.[31]

The XPS analysis of the reduced catalyst 5Ni–5Co-mod alumina was carried out to investigate the various surface species and find their abundance on the catalyst's surface. The XPS peak patterns of Ni 2p and Co 2p orbitals are shown in Fig. 3(a) and (b). The Ni $2p_{3/2}$ XPS spectrum of the catalyst indicates the presence of Ni^{2+} state. Fig. 5(a) shows the two peaks of Ni^{2+}, which corresponds to Ni ($2p_{3/2}$) and Ni ($2p_{1/2}$) at binding energies of 855 eV and 873 eV, respectively. The two satellite peaks, Ni ($2p_{3/2}$) at a binding energy of 861 eV and Ni ($2p_{1/2}$) at 880 eV, for Ni^{2+} are also observed.[33] Fig. 5(b) shows that the binding energies at 781 eV and 796 eV that are ascribed to the spin–orbit coupling Co $2p_{3/2}$ and Co $2p_{1/2}$ confirm the presence of Co^{+2}.[34] The satellite peaks may have originated due to multiple splitting in the spin–orbit energy levels. A ratio of 55 : 44 between nickel and cobalt has been identified from the surface composition studies.

The TEM images for the freshly synthesized 5Ni–5Co-mod alumina catalyst are shown in Fig. 4(a) and (b) represents the TEM images of the reduced form. The images indicate the porous nature of the material before and after the deposition of metal particles. The advantage of the deposition precipitation method of reforming catalyst synthesis is the advantage of the homogenous dispersion of active metal particles.

After SEM analysis, the morphology of the freshly synthesized (5Ni–5Co-mod alumina) catalyst was examined. The image shown in Fig. 4(c) reveals that the trigger has a well-defined flake-like macrostructure.[37]

3.2 Catalyst activity

The catalytic performance for the bireforming of methane was investigated under atmospheric pressure using different catalyst compositions and various reaction conditions using a gas feed composition of $CH_4/CO_2/H_2O$ with a molar ratio of 3/1/2.

On fixing 5% Ni weight percentage and varying the Co composition from 1–5%, all the catalysts have been evaluated for the bireforming of methane in the temperature region of 650–850 °C; the results are demonstrated in Fig. 5. The WHSV is kept constant of 10 L g^{-1} h^{-1} throughout the studies, and the data were collected after 8 h of reaction stabilization. Both CH_4 and CO_2 conversions increase with increasing reaction temperature for all the catalysts. A higher

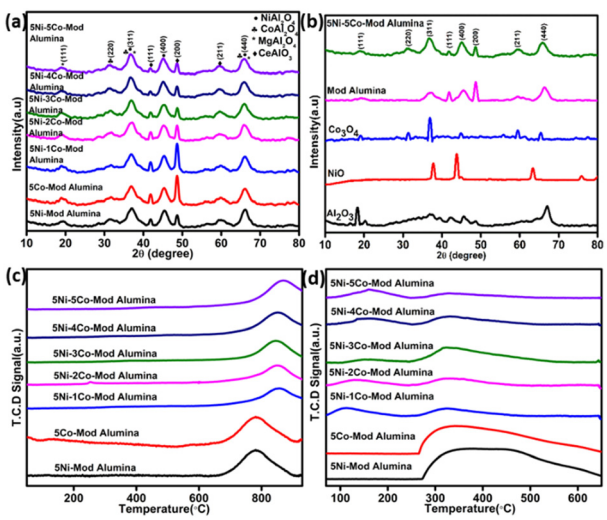

Fig. 2 (a) and (b) XRD profile, (c) H_2-TPR profile, and (d) CO_2-TPD profile of the freshly synthesized catalysts.

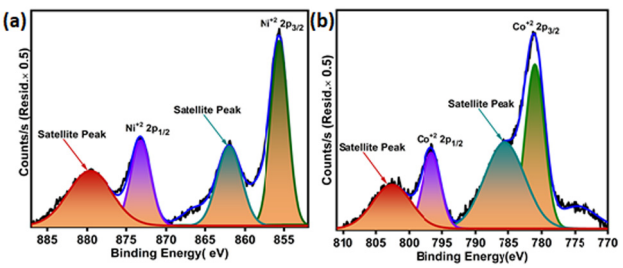

Fig. 3 XPS spectra for (a) Ni 2p and (b) Co 2p in 5Ni–5Co-mod alumina.

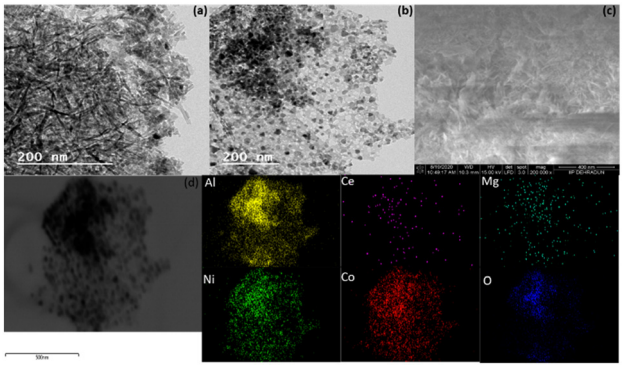

Fig. 4 TEM images for fresh (a) and reduced (b) of 5Ni–5Co-mod alumina. (c) SEM image of 5Ni–5Co-mod alumina. (d) EDX mapping of 5Ni–5Co-mod alumina.

conversion of CH_4 is observed compared to CO_2 for all the catalysts as the water-gas shift reaction ($H_2O + CO \leftrightarrow H_2 + CO_2$), which leads to a higher CH_4 conversion and hence can affect the reaction equilibrium for the bireforming of methane.[38] The catalyst containing 1% Co showed the lowest conversion for both methane and carbon dioxide at all three temperature ranges. For 2%, 3%, and 4% Co, the rate of conversion for CH_4 as well as CO_2 gradually increases with the temperature. Moreover, for all these three catalysts, CH_4 conversion is almost similar at 850 °C. From Fig. 4, it can be observed that the catalyst composition with the equivalent percentage of Ni and Co has a better activity than all. The catalyst can achieve an equal conversion for the feed CH_4 and CO_2 at the highest temperature and be selected for further experimentation. In addition, the H_2/CO ratio also varies with temperature. At 650 °C, the syngas ratio can meet a range between 1.5 to 1.7, whereas at 750 °C, the limit extends from 1.7 to 1.9. However, when the reaction temperature is enhanced to 850 °C, all the catalysts achieve a syngas ratio of nearly 2.

Space velocity is one of the significant parameters for industrial applications as it outlines the volume of the reforming reactor. The 5Ni–5Co-mod alumina catalyst has been taken under investigation for testing the space velocity effect. The catalyst weight has been kept constant, and the flow of reactants is varied to give WHSVs of 10, 20, and 25 L g^{-1} h^{-1}. Experiments were conducted for 8 h at three different temperatures: 650 °C, 750 °C, and 850 °C. Fig. 6 illustrates the catalytic performance of the modified catalyst in terms of CH_4, CO_2 conversion, and H_2/CO ratio as a function of space velocity, taking the steady-state parameter. The studies have shown that by doubling the space velocity from 10 L g^{-1} $h^{-1}$to 20 L g^{-1} h^{-1}, there is little impact on methane conversion at all the temperature ranges, whereas a significant decline in CH_4 conversion was observed when the space velocity increased to 25 L g^{-1} h^{-1}.

Moreover, carbon dioxide conversion decreased by a greater extent at each temperature while the WHSV increased from 10 L g^{-1} h^{-1} to 20 L g^{-1} h^{-1} and 25 L g^{-1} h^{-1}. At the temperature of 650 °C, syngas composition is higher than 2;

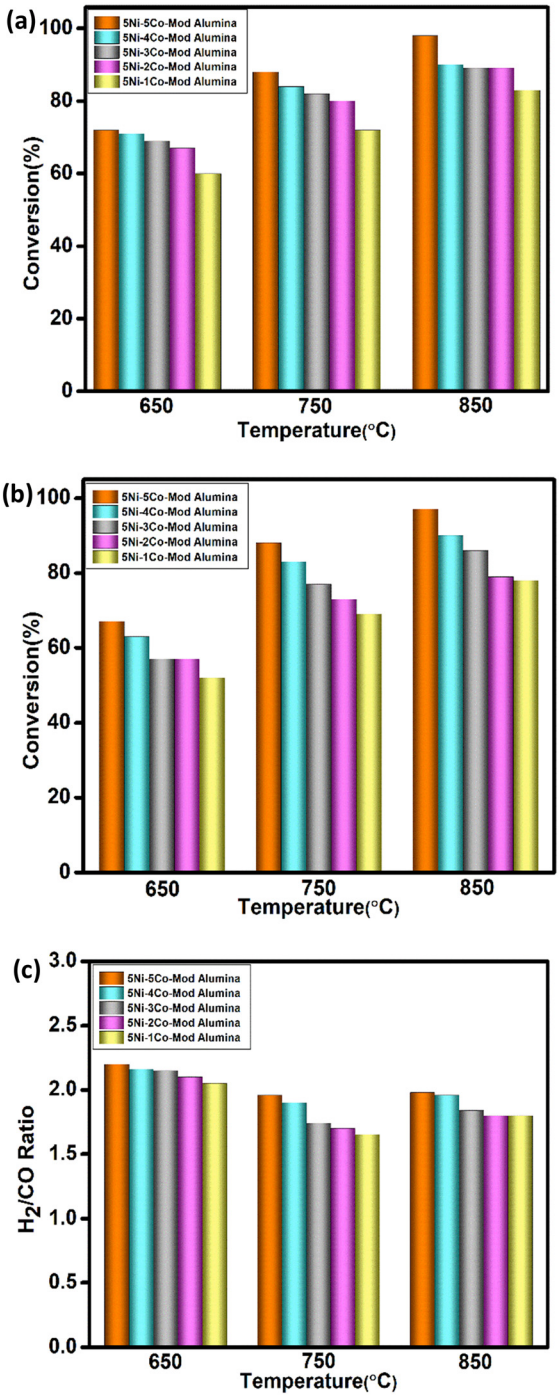

Fig. 5 Effect of temperature over the catalyst compositions at 10 L g^{-1} h^{-1} WHSV and at atmospheric pressure (a) CH_4 conversion (b) CO_2 conversion (c) H_2/CO ratio. Prior to the activity study, the catalyst was reduced at 850 °C with 20% H_2/N_2.

it may be due to the higher CH_4 conversion compared to CO_2. In reforming reactions, the syngas ratio deviates from the optimum value owing to the simultaneous occurring RWGS reaction.[39] RWGS reaction occurs mainly at a lower temperature, which may be one of the reasons for achieving high syngas composition at 650 °C. The syngas ratio has been observed to be decreased down to 2, while the temperature

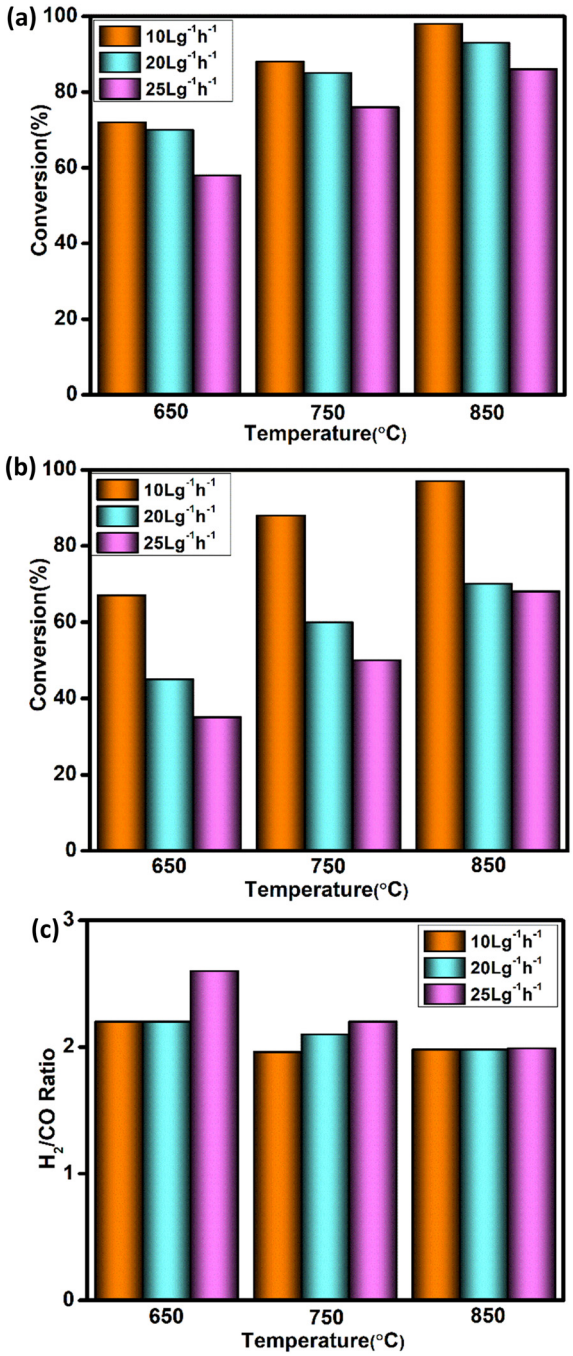

Fig. 6 Effect of space velocity and temperature on the catalytic activity under atmospheric pressure (a) CH_4 conversion (b) CO_2 conversion (c) H_2/CO ratio of 5Ni–5Co-mod alumina. Prior to the activity study, the catalyst was reduced at 850 °C with 20% H_2/N_2.

ranges increased from 650 °C to 750 °C and 850 °C at both WHSV 20 L g^{-1} h^{-1} and 25 L g^{-1} h^{-1}.

Overall, the temperature effect and the space velocity tests signify the excellent performance of the newly designed catalyst system under various reaction conditions. The relatively better behavior at 850 °C suggests that this catalyst can be envisaged as a suitable BRM catalyst (overcoming the coking limitations imposed by thermodynamics). One of the significant advantages of the bireforming of methane is the catalyst shows a negligible amount of coke deposition on the catalyst surface. The presence of steam is reported to be the reason for such catalytic activity.[38] Also, its high activity at relatively demanding space velocity conditions indicates its potential applications in compact units.

To differentiate between monometallic and bimetallic composited, catalyst stability tests have been carried out at temperature 850 °C under atmospheric pressure with WHSV of 10 L g^{-1} h^{-1}, and the results are depicted in Fig. 7(a) and (b) and 8. The feed ratio was kept constant throughout the experiment at 3/1/2 for $CH_4/CO_2/H_2O$, respectively.

For monometallic catalysts, the stability reactions are carried out for 24 h, in which 5N-mod alumina shows excellent activity toward CH_4 conversion, *i.e.*, 98% conversion, but only a 62% conversion is achieved for CO_2 which results a higher syngas ratio of 2.2. Furthermore, cobalt is less active toward methane reforming reaction, and hence 45% CH_4 and 28% CO_2 conversion are achieved with 5C-mod alumina catalyst. Also, the syngas ratio is higher than the desirable ratio of 2, *i.e.*, 2.45. On the other hand, a 500 h reaction is carried out to know the effectiveness of bimetallic system for the bireforming of methane. The catalyst assisted in achieving an excellent conversion of both the feed and exceptional stability without any deactivation throughout the reaction, which is one of the significant advantages of our designed catalyst. The methane conversion reached a steady state with a conversion of 97%. Olah *et al.* using 15% Ni on MgO support could be able to achieve a 70% CH_4 conversion at 830 °C during their 320 h reaction studies.[7] On the other hand, Charisiou *et al.* used Ni–LaCeZr for their longevity reaction studies at 750 °C, and a 40% CH_4 conversion was observed.[40] The second feed carbon dioxide was converted up to 89%, which is lower than methane conversion, which leads to the possibilities of side reactions such as water gas shift reactions, as discussed earlier. Liu *et al.* have also reported a long-term stable catalyst for the BRM reaction. Although the bimetallic Ni–Ir–$MgAl_2O_4$ has shown a stable catalytic activity for a period of 434 h, a high decrease in conversion rate was observed with stepwise pressure increase.[41] The ratio of H_2/CO has a relatively stable value. The catalyst's long-term stability depends on various factors seen during its post-BRM reaction characterization.

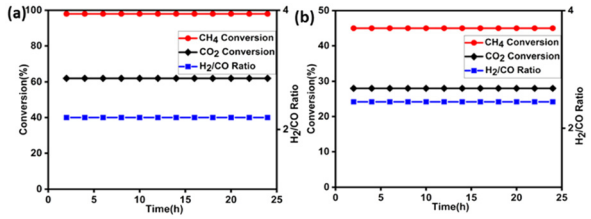

Fig. 7 Effect of time on stream on (a) 5Ni-mod alumina (b) 5Co-mod alumina at 850 °C with WHSV 10 L g^{-1} h^{-1} at atmospheric pressure. Prior to the activity study, the catalyst was reduced at 850 °C with 20% H_2/N_2.

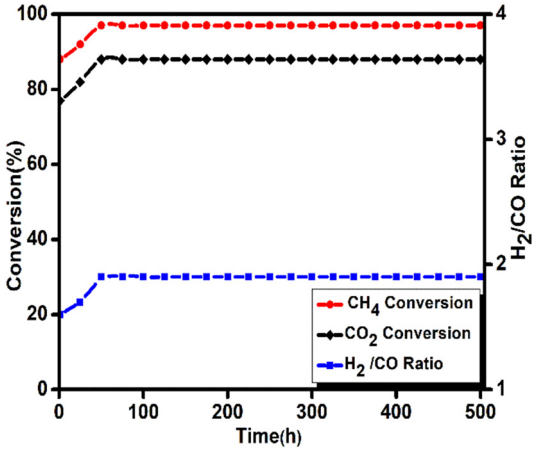

Fig. 8 Effect of time on stream for 5Ni–5Co-mod alumina at 850 °C with WHSV 10 L g^{-1} h^{-1} at atmospheric pressure. Prior to the activity study, the catalyst was reduced at 850 °C with 20% H_2/N_2.

The active particle size, metal dispersion, metal–support interaction, and acidic–basic nature of the supports may be the reason for the high thermal stability.

3.3 Analysis of the spent catalyst

Ni–Co-based catalysts are well-reported for their high activity in reforming reactions. However, metal particle agglomeration and coke deposition are thermodynamically inevitable issues for these catalysts. The catalysts were collected after the reforming reaction and further characterized by XRD, TEM, TPO, TGA, and Raman for determining coke deposition.

A comparative peak pattern of the used catalyst 5Ni-mod alumina, 5Co-mod alumina, and 5Ni–5Co-mod alumina is drawn in Fig. 9. At 2θ, values 45° and 53° confirm the presence of Ni in metallic form, whereas the 2θ values 46° confirmed the Co metallic phase. In each spent catalyst, a peak at 2θ value 26.7° was observed due to the formation of graphitic carbon on the surface of the catalyst (JCPDS Card No. 75-1621),[31] which can be easily removed through the optimized reaction condition. Moreover, the graphitic peak intensity is shown to be high for 5N-mod alumina compared to the rest. The reason may be because Ni has the largest potential for methane cracking and hence allows coke deposition over its surface.

The TEM images of the spent catalysts were recorded for stability reaction at normal atmospheric pressure with 850 °C temperature, and the images are shown in Fig. 10. It has been identified that the porous structure of alumina support is not been disturbed after a long period of reaction studies. Carbon nanotubes are formed near the particles for 5N-mod-alumina. On the other hand, amorphous carbons are observed in the case of 5N–5C-mod alumina and 5C-mod alumina.

O_2-TPO has been performed to endorse the type of carbon deposition over the catalyst surface during activity analysis. The peak profile for the used catalyst after stability test reaction studies is depicted in Fig. 11(a), and the total amount of carbonaceous species deposition was calculated by the peak area formed due to CO_2 release. In case of the monometallic system, 5N-mod alumina, 0.4725 mol g^{-1} coke was deposited and the peak was obtained at 805 °C, which confirmed the presence of crystalline carbon.[42] On the other hand, a total amount of 0.0579 mol g^{-1} at 665 °C was deposited for 5C-mod alumina, which confirms the presence of crystalline coke, but compared to the Ni-based catalyst, it is very less in quantity. The peak centered at 530 °C for 5N–5C mod alumina outlines the formation of graphitic or filament carbon, which can be easily removed with the optimized reaction conditions.[42] During 500 h activity analysis, only a 0.00240 mol g^{-1} of coke was deposited over the spent catalyst. It confirms that the bimetallic catalyst is more prominent toward the catalyst's higher stability and activity in bireforming compared to the monometallic system.

Furthermore, TGA analysis was carried out to quantify the amount of coke deposition, and the peaks are shown in Fig. 11(b). Due to adsorbed water, some portions of weight loss happen at 100 °C. As water vapor is one of the reactant components of the bireforming of methane reaction, it causes the hydroxylation of metal oxides, and hence a weight loss was obtained at 200–400 °C. In addition to this, a 5% weight loss appears for the spent catalyst of 5C-mod alumina and 5N–5C mod alumina above 400 °C, which may be due to the presence of graphitic carbon and then stabilizes at higher temperatures, whereas a total amount of 16% mass loss was

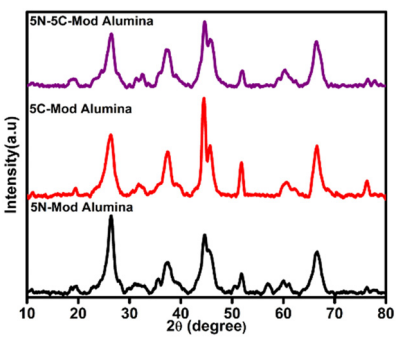

Fig. 9 XRD profile of spent 5N-mod alumina, 5C-mod alumina, and 5N–5C-mod alumina catalysts.

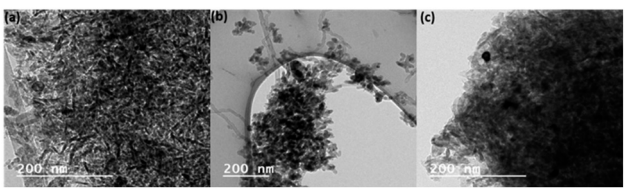

Fig. 10 TEM images of the spent catalyst for (a) 5Ni–5Co-mod alumina, (b) 5Ni-mod alumina, and (c) 5Co-mod alumina.

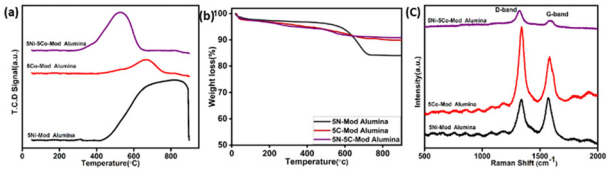

Fig. 11 (a) TPO profile, (b) TGA and (c) Raman analysis of the spent catalysts 5Ni–5Co-mod alumina, 5Co-mod alumina, and 5Ni-mod alumina.

obtained for 5N-mod alumina. The thermogravimetric result is concomitant with the TPO result.

The structure of carbonaceous deposits has been confirmed by the Raman experiment. The spectra confirm the presence of different forms of carbon. Fig. 11(c) illustrates the Raman spectra of the fresh and used catalysts. Two distinct peaks at about 1341 and 1577 cm^{-1} for the used catalyst correspond to the D-band and G-band, respectively. The D-band designates the carbon atoms' breathing mode, correlating the density defects on CNT planes, graphene, or graphitization. The G-band is assigned to sp^2-bonded graphitic carbon. The broadening in the peaks of each spectrum outlines the presence of amorphous carbon.

Although TEM, Raman, and TGA analysis have confirmed the presence of a minimum amount of carbon species, nevertheless, it does not hinder the activity of the catalyst studied in time on stream. This is because some of the catalyst surface-associated carbons act as active sites and are involved in the CO formation reaction.[43]

4 Conclusion

The facile deposition precipitation method has been accomplished to develop a new series of multicomponent stable catalysts for bireforming methane. The catalytic is evolved by tuning the support alumina with the doping of Ce and Mg; later, the active spices Ni was supported synergistically by Co. Adding small quantities of these Ce and Mg dopants regulates the support's acid/base properties, leading to improved CO_2 adsorption and higher oxygen storage capacity. The optimized Ni–Co synergized system is remarkable in the conversion of methane and CO_2 with a constant and highly desirable H_2/CO ratio of about 2 under the optimized reaction conditions. Increasing the temperature increases the conversion level for all the catalysts, magnifying the high endothermicity behavior of bireforming. The catalyst has good thermal stability, which helps sustain a 500 h reaction. The post-reaction catalyst characterization confirmed the presence of a negligible amount of coke, which inadequate to deactivate the catalyst system under the studied conditions. Moreover, this work demonstrates a strategy that paves the path for commercial applications addressing the global challenge of CO_2 mitigation and energy security.

Conflicts of interest

There are no conflicts to declare.

Acknowledgements

S. P. sincerely acknowledges DST New Delhi, India, for fellowship and financial assistance of the Mission Innovation project GAP0016. The Director, CSIR-IIP, is gratefully acknowledged for his kind encouragement. Mr Pranay Rajendra Chandewar is acknowledged due to his technical assistance. The authors thank the analytical science division CSIR-IIP for providing their analytical services.

Notes and references

1 N. Schiaroli, M. Volanti, A. Crimaldi, F. Passarini, A. Vaccari, G. Fornasari, S. Copelli, F. Florit and C. Lucarelli, Biogas to Syngas through the Combined Steam/Dry Reforming Process: An Environmental Impact Assessment, *Energy Fuels*, 2021, **35**(5), 4224–4236.

2 X. Zhao, B. Joseph, J. Kuhn and S. Ozcan, Biogas Reforming to Syngas: A Review, *iScience*, 2020, **23**, 101082.

3 N. H. Elsayed, D. Maiti, B. Joseph and J. N. Kuhn, Precious metal Doped Ni-Mg/ceria-Zirconia Catalysts for Methane Conversion to syngas by low temperature Bi-reforming, *Catal. Lett.*, 2018, **148**, 1003–1013.

4 J. L. Ewbank, L. Kovarik, C. C. Kenvin and C. Sievers, Effect of preparation methods on the performance of Co/Al_2O_3 catalysts for dry reforming of methane, *Green Chem.*, 2014, **2**, 885–896.

5 A. I. Latsiou, O. A. Bereketidou, N. D. Charisiou, A. G. Georgiadis, D. G. Avraam and M. A. Goula, Synthesis and Mathematical Modelling of the Preparation Process of Nickel-Alumina Catalysts with Egg-Shell Structures for Syngas Production via Reforming of Clean Model, Biogas, *Catalysis*, 2022, **12**, 274.

6 S. S. Kapdi, V. K. Vijay, S. K. Rajesh and R. Prasad, Biogas scrubbing, compression and storage: perspective and prospectus in Indian context, *Renewable Energy*, 2005, **30**, 1195–1202.

7 G. A. Olah, A. Goeppert, M. Czaun and G. K. S. Prakash, Bi-reforming of Methane from Any Source with Steam and Carbon Dioxide Exclusively to Metgas (CO–$2H_2$) for Methanol and Hydrocarbon Synthesis, *J. Am. Chem. Soc.*, 2013, **135**, 648–650.

8 R. K. Singha, S. Ghosh, S. S. Acharyya, A. Yadav, A. Shukla, T. Sasaki, A. M. Venezia, C. Pendema and R. Bal, Partial oxidation of methane to synthesis gas over Pt nanoparticles supported on nanocrystalline CeO_2 catalyst, *Catal. Sci. Technol.*, 2016, **6**, 4601–4615.

9 N. Kumar, M. Shojaee and J. J. Spivey, Catalytic bi-reforming of methane: from greenhouse gases to syngas, *Curr. Opin. Chem. Eng.*, 2015, **9**, 8–15.

10 G. A. Olah, A. Goeppert and G. K. S. Prakash, Chemical Recycling of Carbon Dioxide to Methanol and Dimethyl Ether: From Greenhouse Gas to Renewable, Environmentally Carbon Neutral Fuels and Synthetic Hydrocarbons, *J. Org. Chem.*, 2008, **74**, 487–498.

11 N. Kumar, Z. Wang, S. Kanitkar and J. J. Spivey, Methane reforming over Ni-based pyrochlore catalyst: deactivation

studies for different reactions, *Appl. Petrochem. Res.*, 2016, **6**, 201–207.
12 M. Torimoto and Y. Sekine, Effects of alloying for steam or dry reforming of methane: a review of recent studies, *Catal. Sci. Technol.*, 2022, **12**, 3387–3411.
13 Z. Bian, S. Das, M. H. Wai, P. Hongmanorom and S. Kawi, A review on bi-metallic Ni-based catalyst for CO_2 reforming of methane, *ChemPhysChem*, 2017, **18**, 3117–3134.
14 U. S. Mohanty, M. Ali, M. Rizwan, A. Ahmed, A. Al-Yaseri, A. Alireza, A. Keshavarz and S. Iglauer, Current advances in syngas ($CO+H_2$) production through bi-reforming of methane using various catalysts: A review, *Int. J. Hydrogen Energy*, 2021, **46**, 32809–32845.
15 F. Wang, L. Xu, J. Zhang, Y. Zhao, H. Li, H. X. Li, K. Wud, G. Q. Xua and W. Chen, Tuning the metal-support interaction in catalysts for highly efficient methane dry reforming reaction, *Appl. Catal., B*, 2016, **180**, 511–520.
16 M. Shah, T. Das and P. Mondal, Development of nanocrystalline mesoporous Pt promoted Co-based catalysts for carbon dioxide reforming of methane, *Fuel*, 2022, **313**, 122683.
17 S. S. Itkulova, G. D. Zakumbaeva, Y. Y. Nurmakanov, A. A. Mukazhanova and A. K. Yermaganbetova, Syngas production by bireforming of methane over Co-based alumina-supported catalysts, *Catal. Today*, 2014, **224**, 194–198.
18 S. A. Shin, Y. S. Noh, G. H. Hong, J. I. Park, H. T. Song, K.-Y. Lee and D. J. Moon, Dry reforming of methane over Ni/ZrO_2–Al_2O_3 catalysts: effect of preparation methods, *J. Taiwan Inst. Chem. Eng.*, 2018, **90**, 25–32.
19 R. D. Gonzalez, T. Lopez and R. Gomez, Sol–gel preparation of supported metal catalysts, *Catal. Today*, 1997, **35**(3), 293–317.
20 S. M. Sajjadi, M. Haghighi and F. Rahmani, Dry reforming of greenhouse gases CH_4/CO_2 over MgO-promoted $Ni–Co/Al_2O_3$–ZrO_2 nanocatalyst: effect of MgO addition via sol-gel method on catalytic properties and hydrogen yield, *J. Sol-Gel Sci. Technol.*, 2014, **70**, 111–124.
21 L. Xu, H. Song and L. Chou, Ordered mesoporous MgO–Al_2O_3 composite oxides supported Ni-based catalysts for CO_2 reforming of CH_4: effects of basic modifier and mesopore structure, *Int. J. Hydrogen Energy*, 2013, **38**(18), 7307–7325.
22 T. Stroud, T. J. Smith, E. Le Saché, J. L. Santos, M. A. Centeno, H. Arellano-Garcia, J. A. Odriozol and T. R. Reina, Chemical CO_2 recycling via dry and bi reforming of methane using $Ni-Sn/Al_2O_3$ and $Ni-Sn/CeO_2$-Al_2O_3 catalysts, *Appl. Catal., B*, 2018, **224**, 125–135.
23 J. Wei and E. Iglesia, Isotopic and kinetic assessment of the mechanism of reactions of CH_4 with CO_2 or H_2O to form synthesis gas and carbon on nickel catalysts, *J. Catal.*, 2004, **224**, 370–383.
24 A. L. A. Marinho, F. S. Toniolo, F. B. Noronha, F. Epron, D. Duprez and N. Bion, Highly active and stable Ni dispersed on mesoporous CeO_2-Al_2O_3 catalysts for production of syngas by dry reforming of methane, *Appl. Catal., B*, 2021, **281**, 119459.
25 K. Han, W. Yu, L. Xu, Z. Deng, H. Yue and F. Wang, Reducing carbon deposition and enhancing reaction stability by ceria for methane dry reforming over $Ni@SiO_2@CeO_2$ catalyst, *Fuel*, 2021, **291**, 120182.
26 S. Wang and G. Q. Lu, Role of CeO_2 in Ni/CeO_2–Al_2O_3 catalysts for carbon dioxide reforming of methane, *Appl. Catal., B*, 1998, **19**, 267–277.
27 S. Das, M. Sengupta, A. Bag, M. Shah and A. Bordoloi, Facile synthesis of highly disperse Ni-Co nanoparticles over mesoporous silica for enhanced methane dry reforming, *Nanoscale*, 2018, **10**, 6409–6425.
28 S. M. Morris, P. F. Fulvio and M. Jaroniec, Ordered Mesoporous Alumina-Supported Metal Oxides, *J. Am. Chem. Soc.*, 2008, **130**, 15210–15216.
29 S. Das, M. Sengupta, J. Patel and A. Bordoloi, A study of the synergy between support surface properties and catalyst deactivation for CO_2 reforming over supported Ni Nanoparticles, *Appl. Catal., A*, 2017, **545**, 113–126.
30 M. D. Donohue and G. L. Aranovich, Classification of Gibbs adsorption isotherms, *Adv. Colloid Interface Sci.*, 1998, **76**, 137–152.
31 S. Das, S. Thakur, A. Bag, M. S. Gupta, P. Mondal and A. Bordoloi, Support interaction of Ni nanocluster-based catalysts applied in CO_2 reforming, *J. Catal.*, 2015, **330**, 46–60.
32 O. A. Bereketidou and M. A. Goula, Biogas reforming for syngas production over nickel supported on ceria–alumina catalysts, *Catal. Today*, 2012, **195**, 93–100.
33 H. Singha, A. Raia, R. Yadav and A. K. Sinha, Glucose hydrogenation to sorbitol over unsupported mesoporous Ni/NiO catalyst, *Mol. Catal.*, 2018, **451**, 186–191.
34 R. K. Singha, S. Das, M. Pandey, S. Kumar, R. Bal and A. Bordoloi, Ni nanocluster on modified CeO_2–ZrO_2nanoporous composite for tri-reforming of methane, *Catal. Sci. Technol.*, 2016, **6**, 7122–7136.
35 J. R. Rostrup-Nielsen, Catlytic steam reforming, *Catal. Sci. Technol.*, 1984, **5**, 1–117.
36 K. S. Park, M. H. Jeong and J. W. Bae, Synergy Effects of Cobalt Oxides on Ni/Co-Embedded Al_2O_3 for Hydrogen-Rich Syngas Production by Steam Reforming of Propane, *Catalysts*, 2020, **10**, 461.
37 A. Parmaliana, F. Arena, F. Frusteri and N. Giordano, Temperature-programmed reduction study of NiO–MgO interactions in magnesia-supported Ni catalysts and NiO–MgO physical mixture, *J. Chem. Soc., Faraday Trans.*, 1990, **86**, 2663.
38 A. S. Farooqi, M. Yusuf, N. A. M. Zabidi, R. Saidur, M. U. Shahid, B. V. Ayodele and B. Abdullah, Hydrogen-rich syngas production from bi-reforming of greenhouse gases over zirconia modified Ni/MgO catalyst, *Int. J. Energy Res.*, 2022, **46**(3), 2529–2545.
39 S. Singh, M. B. Bahari, B. Abdullah, T. T. P. Phuong, D. Q. Truong, N. D. Vo and A. A. Adesina, Bi-reforming of methane on Ni/SBA-15 catalyst for syngas production: Influence of feed composition, *Int. J. Hydrogen Energy*, 2018, **43**, 17230–17243.
40 N. D. Charisiou, G. Siakavelas, L. Tzounis, V. Sebastian, A. Monzon, M. A. Baker, S. J. Hinder, K. Polychronopoulou, I. V. Yentekakis and M. A. Goula, An in depth investigation of

deactivation through carbon formation during the biogas dry reforming reaction for Ni supported on modified with CeO_2 and La_2O_3 zirconia catalysts, *Int. J. Hydrogen Energy*, 2018, **43**(41), 18955–18976.

41 Z. Liu, F. Gao, Y. A. Zhu, Z. Liu, K. Zhu and X. Zhou, Bi-reforming of methane with steam and CO_2 under pressurized conditions on a durable Ir–Ni/$MgAl_2O_4$ catalyst, *Chem. Commun.*, 2020, **56**, 13536–13539.

42 H. M. Nguyen, G. H. Pham, M. Tade, C. Phan, R. Vagnoni and S. Liu, Microwave-Assisted Dry and Bi-reforming of Methane over M–Mo/ TiO_2 (M = Co, Cu) Bimetallic Catalysts, *Energy Fuels*, 2020, **34**, 7284–7294.

43 A. L. A. Marinho, R. C. Rabelo-Neto, F. Epron, N. Bion, F. S. Toniolo and F. B. Noronha, Embedded Ni nanoparticles in $CeZrO_2$ as stable catalyst for dry reforming of methane, *Appl. Catal., B*, 2020, **268**, 118387.